Flow-Driven Waves and Phase-Locked Self-Organization in Quasi-One-Dimensional Colonies of *Dictyostelium discoideum*

A. Gholami,[1] O. Steinbock,[4] V. Zykov,[1] and E. Bodenschatz[1,2,3]
[1]*Max Planck Institute for Dynamics and Self-Organization, Am Fassberg 17, D-37077 Göttingen, Germany*
[2]*Institute for Nonlinear Dynamics, University of Göttingen, D-37073 Göttingen, Germany*
[3]*Laboratory of Atomic and Solid-State Physics and Sibley School of Mechanical and Aerospace Engineering, Cornell University, Ithaca, New York 14853, USA*
[4]*Department of Chemistry and Biochemistry, Florida State University, Tallahassee, Florida 32306-4390, USA*
(Received 14 August 2014; published 6 January 2015)

We report experiments on flow-driven waves in a microfluidic channel containing the signaling slime mold *Dictyostelium discoideum*. The observed cyclic adenosine monophosphate (cAMP) wave trains developed spontaneously in the presence of flow and propagated with the velocity proportional to the imposed flow velocity. The period of the wave trains was independent of the flow velocity. Perturbations of flow-driven waves via external periodic pulses of the signaling agent cAMP induced 1:1, 2:1, 3:1, and 1:2 frequency responses, reminiscent of Arnold tongues in forced oscillatory systems. We expect our observations to be generic to active media governed by reaction-diffusion-advection dynamics, where spatially bound autocatalytic processes occur under flow conditions.

DOI: 10.1103/PhysRevLett.114.018103 PACS numbers: 87.18.Hf, 82.39.Rt, 82.40.Ck

Transport-coupled nonlinear dynamics is fundamental to most types of spatiotemporal self-organization. The rich physics of these processes is not only of basic interest, but holds the key to understanding biological phenomena such as cell motion, embryogenesis, dynamical diseases, and patterns in bacterial systems [1–5]. Important examples are found in reaction-diffusion media, which have provided valuable insights into systems as diverse as the patterned shells of mollusks, neuronal networks, and the human heart [6,7]. Usually in these reaction-diffusion systems transport coupling in the form of molecular diffusion or diffusionlike electric processes is considered. In contrary, transport coupling by fluid flow has received little attention, with experiments focusing mainly on the Belousov-Zhabotinsky (BZ) reaction [8–11]. Here we show that reaction-diffusion advection has fundamental consequences for biological systems that use solutes as signaling agents.

In this Letter, we present experimental results on flow-driven waves in the signaling of the amoebae *Dictyostelium discoideum* (*D.d.*). This organism, naturally occurring in forest soil, is an important model system for the study of chemotaxis, cell differentiation, and morphogenesis [12]. When starved, 10^5–10^6 individual cells signal each other and form multicellular centimeter-scale Voronoi domains. The corresponding wave sources in each domain then act as aggregation centers, which eventually transform into millimeter long slugs and finally into fruiting bodies bearing spores for long-term survival and long-range dispersal. Underlying the signaling of *D.d.* are diffusive waves of the extracellular messenger cyclic adenosine monophosphate (cAMP), which are amplified via secretion of cAMP by individual cells when they are exposed to extracellular cAMP [13–15]. In the natural environment, populations of starving *D.d.* may experience fluid flows that will profoundly alter the wave generation processes as we show here. Although in nature these wave processes occur in three dimensions, a first understanding may be gained in a quasi-1D geometry.

Our experiments investigate spatial-temporal dynamics of a uniformly distributed population of *D.d.* cells in a flow-through narrow microfluidic channel. As shown in Fig. 1, the starved amoebae are attached to the surface of the channel and exposed to an external fluid flow that advects cAMP molecules downstream. This transport anisotropy in the extracellular medium induced macroscopic wave trains that differ profoundly from conventional excitation waves in this system. Moreover, with this setup we injected cAMP pulses periodically and studied the phase-locking properties of the system.

The *D.d.* cells (cell line AX2) were grown in HL5 medium, harvested in the exponential growth phase, and starved for 4 h in a phosphate buffer under shaking [17]. The cells with the density of 4×10^7 cells/ml were loaded into a straight microfluidic device approximately 200 cells wide, 3000 cells long, and 10 cells high (30 mm × 2 mm × 100 μm) that we produced from polydimethylsiloxane (PDMS) and glass using soft lithography [18]. Cells were allowed to settle for 15 min before a laminar flow of phosphate buffer was started [Fig. 1(a)]. cAMP wave patterns are indirectly inferred based on cell response visualized by dark-field microscopy. Since the change of the scattered light reflects the cell shape change associated with cAMP, we indirectly observe the propagating waves of cAMP [19–22].

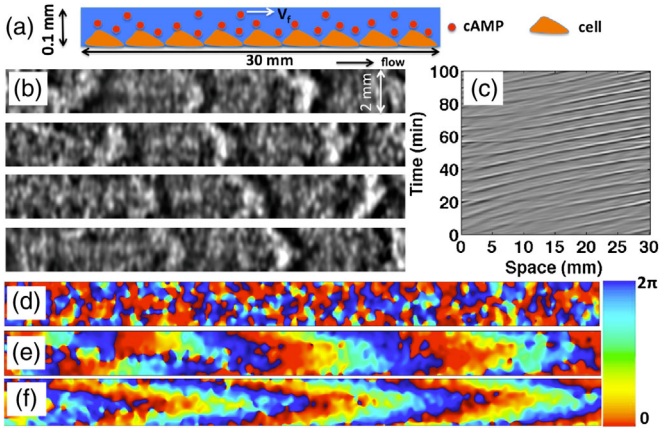

FIG. 1 (color online). (a) A schematic side view of the experimental setup. Buffer was flowing with an average velocity $V_f = 2$ mm/ min from left to the right transporting cAMP molecules downstream. (b) Top view of flow-driven waves obtained by subtracting two successive images (20 s time interval) of the channel and bandpass filtered, where large structures are filtered down to 3.5 mm and small structures up to 0.294 mm. The time interval between the images is 100 s (see Supplemental Movie 2 [16]). (c) Corresponding space-time plot from averaging over the full width of the channel at each time. (d) Phase maps of the observed spatial-temporal oscillations before and (e) during flow-driven wave propagation. (f) At larger flow velocity of $V_f = 5$ mm/ min, deformations of the wave fronts are increased (see Supplemental Movie 3 [16]).

In the absence of flow, spiral or target patterns emerge at different locations along the channel (see Supplemental Material, Movie 1 [16]). This is in contrast with flow-driven waves, where waves originate at the inlet region of the device, as shown in Fig. 1. Figure 1(b) shows an example of flow-driven waves for the average flow velocity of $V_f = 2$ mm/ min (see Supplemental Material, Movie 2 [16]). The four successive snapshots reveal bright bands propagating in the flow direction. The image contrast reflects the shape changes of the cells. The light bands correspond to high concentrations of cAMP and consist of elongated chemotactic cells while in the dark bands the cAMP concentration is small and cells remain round [19–22]. The flow velocities were chosen to be below the shear stresses known to be necessary for mechanotaxis [23] or cell-substrate detachment [24]. In all experiments we observed that flow-driven waves (i) developed simultaneously over the entire channel, (ii) were propagating solely in the flow direction, and (iii) had curved wave fronts.

Figure 1(c) shows the space-time plot for $V_f = 2$ mm/ min with diagonal bands giving the average wave velocity V_w and the wavelength λ_w (here 1.43 mm/ min and 8.33 mm, respectively). We obtain the power spectrum of the signal and the leading frequency by computing the discrete Fourier transform (DFT). The DFT of the averaged light intensity $\langle I(t)\rangle_{x,y}$ is defined as

$$I(k) = \frac{1}{N}\sum_{n=1}^{N}\langle I(n)\rangle_{x,y}\exp\left(2\pi i\frac{(n-1)(k-1)}{N}\right), \quad (1)$$

where N is the total number of frames, and averages are taken over spatial regions of interest. During wave propagation, $I(k)$ has the dominant peak at $k_{\max}$ which corresponds to the period of $T = \Delta t * N/(k_{\max} - 1)$, where Δt is the time between two successive frames. The power spectrum analysis of the signal yielded $T = 6.8 \pm 0.18$ min, which matches the typical oscillation period of extracellular cAMP in spatially homogeneous, well-stirred systems [21,25]. Figures 1(d)–1(f) show the spatial (pixelwise) phase map as calculated at the dominant frequency in the power spectrum. A nearly structureless map is observed initially for 1–2 h before wave initiation [Fig. 1(d)]. The average parabolic deformation of the wave front after the onset of wave propagation is characterized in Fig. 1(e). Our results also reveal that these deformations increase in amplitude with increasing flow velocities (see Fig. 1(f) and Supplemental Material, Movie 3 [16]) and eventually cause the single wave front to extend over the entire length of the channel (Supplemental Material, Movie 4 [16]).

Experiments at different flow rates show that, within the experimental error, both V_w and λ_w are proportional to the flow velocity while the period T is practically velocity independent (Fig. 2). This differs profoundly from the situation in the absence of fluid flow, where the pacemaker of a given wave pattern (e.g., a target pattern or spiral rotor) determines the wave period based on its local characteristics. For a given preparation, these periods can vary by up to 33% [25]. The wave velocity and respective wavelength are then determined by the system's dispersion relation $V_w(T)$, which depends nearly exclusively on the underlying reaction network and cAMP diffusion. Accordingly, the data in Fig. 2 provide strong evidence for the presence of flow-driven waves.

To investigate the dynamical selection of flow-driven waves, we perturbed the system by periodically injecting cAMP pulses at the upstream end of the channel. We performed experiments with pulses of fixed concentration

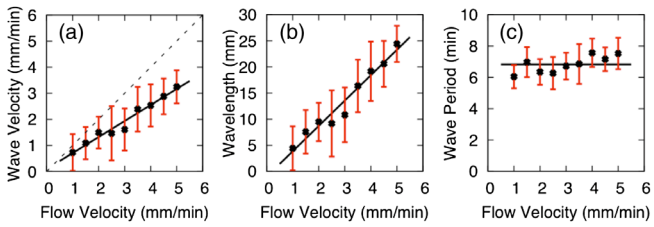

FIG. 2 (color online). Experimental data on the dependences of (a) wave velocity, (b) wavelength, and (c) wave period on the average flow velocity. Continuous lines represent (a),(b) least-squares fits assuming proportionality and (c) the average period. The dashed line describes equal wave and flow velocities.

of external cAMP (0.5 μM). This concentration was found to produce well-developed responses and is the lower bound of the range previously used for no-flow experiments [26]. The injection periods T_p were 2 min $\leq T_p \leq$ 16 min. The volume of cAMP in each injection was 0.25 μl with the injection rate of 5 μl/ min and pulse duration of 3 s. At the channel entrance a pulse of cAMP elicited a fast contraction response in the shape of the cells. This well-known "cringe" response [27,28] was locked to the perturbation period and propagated downstream with the flow velocity. Initially, the response was observed to decay towards the end of the channel. However with time progressively, after about 70 min, we observed the appearance of flow-driven waves in the middle of the channel that propagated towards its end.

Figure 3 shows examples of the spatiotemporal responses. We observed zones of regular and irregular dynamics at the distal end of the channel. For regular responses, we found a $L:M$ resonance, where L and M are integers. Examples can be seen in Figs. 3(a), (b), (c), and (e) (as well as Fig. 4), which show a 3:1, 2:1, 1:1, and 1:2 resonance, respectively. We observed 1:1 responses for a wide range of stimulus periods between 4 and 8 min. An example of irregular pattern with complex oscillations is shown in Figs. 3(d) and 4(d), where the injection period of cAMP was 9 min. As T_p decreased to 3 min, first a 1:1 propagated cringe response is observed over the entire length of the channel. After 40 min, flow-driven waves developed away from the injection site and cringe waves died out at the middle of the channel. However, after 70 min, a 1:1 cringe response was replaced downstream by a 2:1 response at the distal end of the channel, where every second wave was blocked [Figs. 3 and 4(b)]. A transition to propagation block was also observed at faster injection periods, namely $T_p = 2$ min, where a transition to a stable 3:1 response occurred [Figs. 3 and 4(a)]. Furthermore, at very slow stimulus period of $T_p = 16$ min, a 1:2 response was observed [Figs. 3 and 4(e)].

Our experimental results can clearly be interpreted as movements through adjacent Arnold tongues [29] caused by changes in the driving frequency $1/T_p$. Hence, responses are phase locked only for those parameter values that fall inside an Arnold tongue. Period values outside Arnold tongues give irregular behavior and show no synchronization. This is consistent with further experiments that vary the concentration of the cAMP pulses, which are currently under way.

Flow-driven waves may have also important biological consequences on the aggregation dynamics of the *D.d.* cells. Our observations show that the wave's persistence length is much larger than without flow. As cells are chemotactic one would expect that they all migrate upstream to the injection or wave self-generation site. As the time for this migration would be too long one would expect, in the absence of any other mechanisms, that

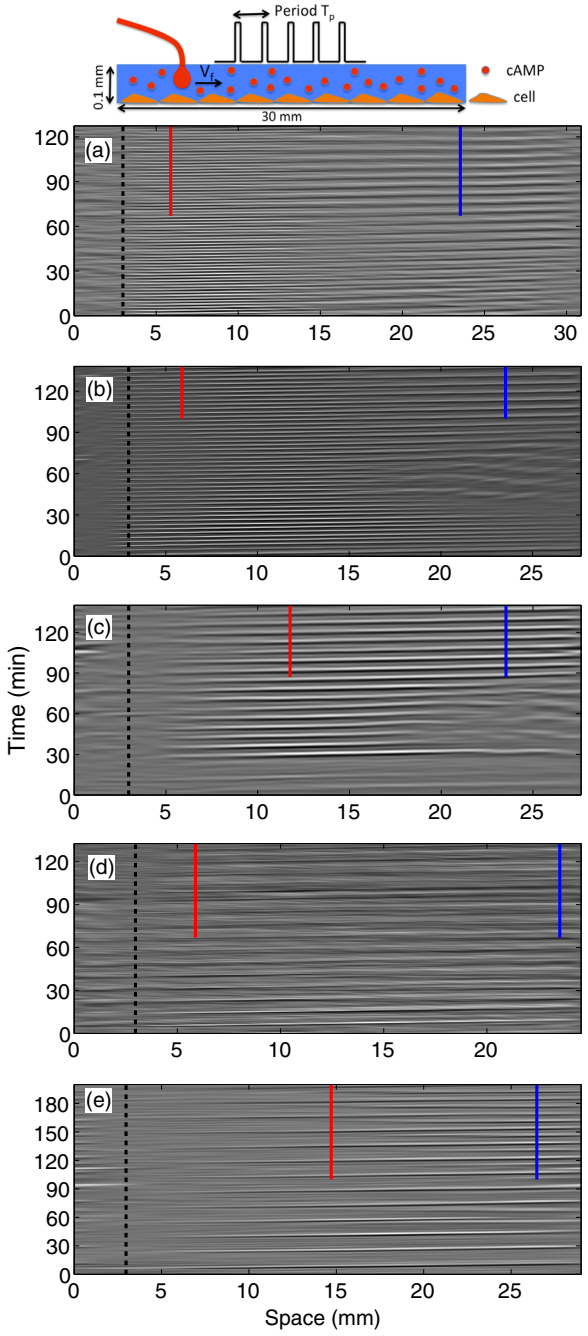

FIG. 3 (color online). The modified experimental setup to study response in a colony of homogeneously distributed *D.d.* cells in a flow-through microfluidic channel with periodic cAMP injections. (a) 3:1 response observed away from the perturbation position with cAMP injection period of 2 min. (b) 2:1 response for the injection period of 3 min. (c) 1:1 entrainment observed in an experiment with cAMP stimulus injected every 7 min. (d) Transition to irregular pattern is observed at the injection period of 9 min. (e) In the case of the slow rate of cAMP injection, namely, every 16 min, 1:2 response is developed at the distal end of the channel. The dashed black line denotes the injection site of cAMP and the intensity versus time plots in Fig. 4 are plotted along the red and the blue lines in the corresponding space-time plots.

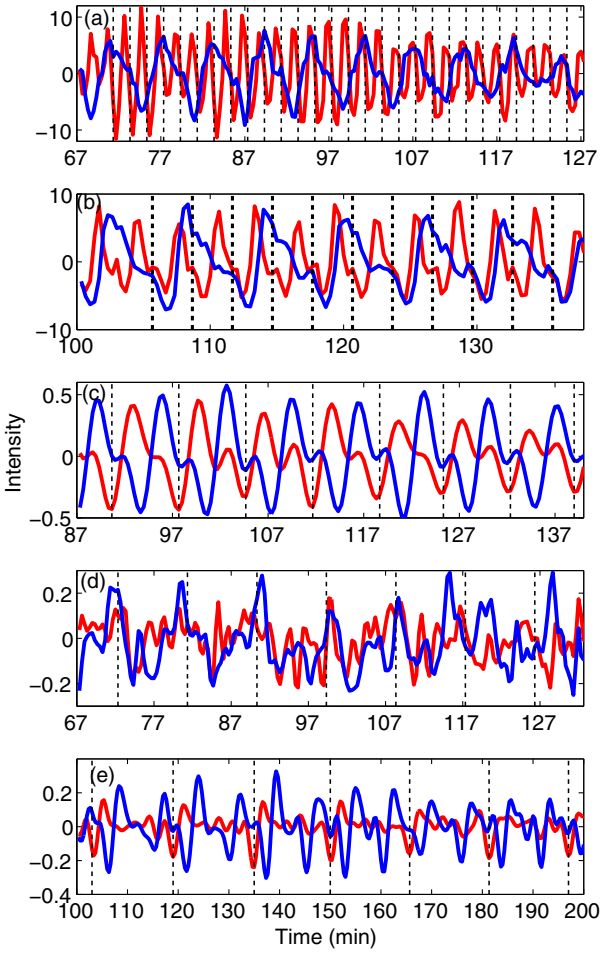

FIG. 4 (color online). Various types of oscillations in response to repetitive periodic stimuli of cAMP shown as the black dashed lines. The red and blue colors correspond to the intensity plots along the red and blue lines in Fig. 3. From the top trace to the bottom trace, the stimulus intervals are 2, 3, 7, 9, and 16 min, respectively.

no aggregation clusters should form. In both cases, no cell streaming was observed. This is perplexing at first sight, as in the natural environment *D.d.* is typically found in forest soils, where fluid flows are very common and can be expected to influence the aggregation dynamics along the lines observed here. Notice that rainwater speeds in soils can vary from near zero to values 1 order of magnitude larger than flow rates in our study [30]. At those large speeds we observed cells to be washed out of the device.

To investigate this question further, we performed experiments in which the flow is maintained well into the culmination phase of the life cycle. We then analyzed the spatial coordinates of the cell aggregates and surprisingly found a random distribution for most of the experiments. Furthermore, qualitative inspection showed the same for flow-free aggregates (Fig. 5). In our experiments waves appear 3–6 h after starvation. During this time, the cell motion due to chemotaxis is weak [31] and did not

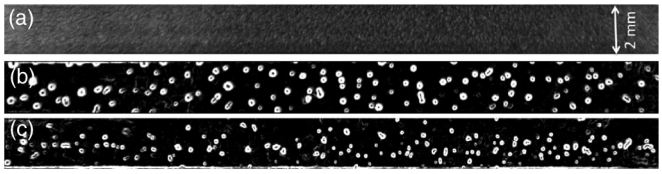

FIG. 5. (a) Uniform *D.d.* amoebae distribution at the beginning of experiment in a flow-through microfluidic channel ($V_f = 15$ mm/ min). (b) Aggregation centers after 8 h starvation in the presence of flow-driven waves show a random distribution along the channel (see Supplemental Movie 5 [16]). (c) In a few experiments (3 out of 50), the aggregation centers are distributed around the middle of the channel.

produce patterns in cell density. Later, after 8 h, cells aggregate into small clumps as shown in Fig. 5(b). We also observed that the flow structure itself can influence aggregation, for instance, due to the parabolic front shape one would expect that cells would aggregate preferentially in the middle of the channel. This we observed in a few cases as shown in Fig. 5(c). Clearly more detailed studies are needed to explore these aggregation patterns, why streaming does not occur in the channel, and how it couples to the flow.

In conclusion, we have shown that a flow of extracellular cAMP through a field of signaling *D.d.* cells can lead to wave propagation. This phenomenon is reproducible and observed for a wide range of flow rates as well as cell densities. Flow-driven waves are also observed in the autocatalytic Belousov-Zhabotinsky (BZ) reaction, where differential flow destabilizes an otherwise spatially homogeneous state of the system. A differential flow induced chemical instability (DIFICI) was originally predicted by Rovinsky and Menzinger [8,9] and later observed in the BZ reaction [10,32]. DIFICI shares some similarities with the Turing instability [33] for which differential diffusion spatially disengages antagonistic species. The DIFICI, however, is free from the restrictions of molecular size on diffusion coefficients and should thus exist in a wide variety of chemical, physical, and biological systems. Nevertheless, up to now the BZ reaction has remained as the only unambiguous experimental example, although flow-driven transport instabilities have been hypothesized as factors during biological morphogenesis [11] and population dynamics [34] for a long time. The system presented here shares many similarities with DIFICI, but there are also important differences. For instance, in the absence of the flow, signaling *D.d.* amoebae represent a system under continuous development, they synchronize and show formation and propagation of spiral waves, while the BZ systems'investigated homogeneous solutions were stable. In addition, in a convectively unstable system, like DIFIC, the inlet perturbation drifts with the flow and grows over a length scale called the "healing length". This we did not observe in our experiments with *D.d.* cells.

From a general perspective, *D.d.* presents itself as a very suitable model system to further elucidate the distribution of the cell populations under the influence of differential flow [35] and investigations in this direction are under way in our laboratory.

We thank N. Oikawa, C. Westendorf, B. Utter, M. Naghipour, A. Sharo, and K. Schneider. A. G. was supported by the Dorothea-Schlözer scholarship of Georg-August-Universität Göttingen, Germany. O. St. acknowledges support provided by the Alexander von Humboldt Foundation and the National Science Foundation (Grant No. CHE-1213259).

[1] D. Y. Shao, H. Levine, and W. J. Rappel, Proc. Natl. Acad. Sci. U.S.A. **109**, 6851 (2012).
[2] N. W. Goehring, P. K. Trong, J. S. Bois, D. Chowdhury, E. M. Nicola, A. A. Hyman, and S. W. Grill, Science **334**, 1137 (2011).
[3] S. Luther *et al.*, Nature (London) **475**, 235 (2011).
[4] P. Stoodley, Z. Lewandowski, J. D. Boyle, and H. M. Lappin-Scott, Environ. Microbiol. **1**, 447 (1999).
[5] L. J. Shimkets and D. Kaiser, J. Bacteriol. **152**, 451 (1982).
[6] J. D. Murray, *Mathematical Biology* (Springer-Verlag, Berlin, 1989).
[7] A. T. Winfree, *The Geometry of Biological Time* (Springer, New York, 2010).
[8] A. B. Rovinsky and M. Menzinger, Phys. Rev. Lett. **69**, 1193 (1992).
[9] A. B. Rovinsky and M. Menzinger, Phys. Rev. Lett. **72**, 2017 (1994).
[10] A. B. Rovinsky and M. Menzinger, Phys. Rev. Lett. **70**, 778 (1993).
[11] M. Kaern, M. Menzinger, R. Satnoianub, and A. Hunding, Faraday Discuss. **120**, 295 (2001).
[12] R. L. Chisholm and R. A. Firtel, Nat. Rev. Mol. Cell Biol. **5**, 531 (2004).
[13] A. V. Holden, M. Markus, and H. G. Othmer, *Nonlinear Wave Processes in Excitable Media* (Plenum Press, New York, 1989).
[14] S. Saran, M. E. Meima, E. Alvarez-Curto, K. E. Weening, D. E. Rozen, and P. Schaap, J. Muscle Res. Cell Motil. **23**, 793 (2002).
[15] M. T. Laub and W. F. Loomis, Mol. Biol. Cell **9**, 3521 (1998).
[16] See Supplemental Material at http://link.aps.org/supplemental/10.1103/PhysRevLett.114.018103 for movies.
[17] A. J. Warren, W. D. Warren, and E. C. Cox, Genetics **83**, 25 (1976).
[18] G. M. Whitesides, E. Ostuni, S. Takayama, X. Jiang, and D. E. Ingber, Annu. Rev. Biomed. Eng. **3**, 335 (2001).
[19] F. Alcantara and M. Monk, J. Gen. Microbiol. **85**, 321 (1974).
[20] J. D. Gross, M. J. Peacey, and D. J. Trevan, J. Cell Sci. **22**, 645 (1976).
[21] P. N. Devreotes, M. J. Potel, and S. A. MacKay, Dev. Biol. **96**, 405 (1983).
[22] P. N. Devreotes and K. Tomchik, Science **212**, 443 (1981).
[23] E. Décavé, D. Rieu, J. Dalous, S. Fache, Y. Bréchet, B. Fourcade, M. Satre, and F. Bruckert, J. Cell Sci. **116**, 4331 (2003).
[24] E. Décavé, D. Garrivier, Y. Breche, B. Fourcade, and F. Bruckert, Biophys. J. **82**, 2383 (2002).
[25] F. Siegert and C. J. Weijer, J. Cell Sci. **93**, 325 (1989).
[26] J. Rietdorf, F. Siegert, and C. J. Weijer, Dev. Biol. **204**, 525 (1998).
[27] R. P. Futrelle, J. Traut, and W. G. McKee, J. Cell Biol. **92**, 807 (1982).
[28] T. Tani and Y. Naitoh, J. Exp. Biol. **202**, 1 (1999).
[29] V. I. Arnold, Russ. Math. Surv. **38**, 215 (1983).
[30] M. P. Mosley, J. Hydrol. **55**, 65 (1982).
[31] D. Wessels *et al.*, Eukaryotic Cell **3**, 646 (2004).
[32] R. Toth, A. Papp, V. Gaspar, J. H. Merkin, S. K. Scott, and A. F. Taylor, Phys. Chem. Chem. Phys. **3**, 957 (2001).
[33] A. Turing, Phil. Trans. R. Soc. B **237**, 37 (1952).
[34] H. Malchow, Ecol. Model. **82**, 257 (1995).
[35] J. M. Garcia and Z. Neufeld, Phys. Rev. E **80**, 061902 (2009).